ORIGINAL ARTICLE

Joint Multi-modal Parcellation of the Human Striatum: Functions and Clinical Relevance

Xiaojin Liu[1,2] · Simon B. Eickhoff[1,2] · Felix Hoffstaedter[1,2] · Sarah Genon[1,2] ·
Svenja Caspers[3,4] · Kathrin Reetz[6] · Imis Dogan[5,6] · Claudia R. Eickhoff[3,7] ·
Ji Chen[1,2] · Julian Caspers[3,8] · Niels Reuter[1,2] · Christian Mathys[8,9] ·
André Aleman[10] · Renaud Jardri[11] · Valentin Riedl[12] · Iris E. Sommer[9] ·
Kaustubh R. Patil[1,2]

Abstract The human striatum is essential for both low- and high-level functions and has been implicated in the pathophysiology of various prevalent disorders, including Parkinson's disease (PD) and schizophrenia (SCZ). It is known to consist of structurally and functionally divergent subdivisions. However, previous parcellations are based on a single neuroimaging modality, leaving the extent of the multi-modal organization of the striatum unknown. Here, we investigated the organization of the striatum across three modalities—resting-state functional connectivity, probabilistic diffusion tractography, and structural covariance—to provide a holistic convergent view of its structure and function. We found convergent clusters in the dorsal, dorsolateral, rostral, ventral, and caudal striatum. Functional characterization revealed the anterior striatum to be mainly associated with cognitive and emotional functions, while the caudal striatum was related to action execution. Interestingly, significant structural atrophy in the rostral and ventral striatum was common to both PD and SCZ, but atrophy in the dorsolateral striatum was specifically attributable to PD. Our study revealed a cross-modal

✉ Kaustubh R. Patil
k.patil@fz-juelich.de

1   Institute of Neuroscience and Medicine (INM-7, Brain and Behaviour), Research Centre Jülich, Jülich, Germany

2   Institute of Systems Neuroscience, Heinrich Heine University Düsseldorf, Düsseldorf, Germany

3   Institute of Neuroscience and Medicine (INM-1), Research Centre Jülich, 52428 Jülich, Germany

4   Institute for Anatomy I, Medical Faculty, Heinrich Heine University Düsseldorf, 40225 Düsseldorf, Germany

5   Jülich Aachen Research Alliance-BRAIN (JARA) Institute of Molecular Neuroscience and Neuroimaging, Forschungszentrum Jülich, Rheinisch Westfällische Technische Hochschule (RWTH) Aachen University, 52074 Aachen, Germany

6   Department of Neurology, Rheinisch Westfällische Technische Hochschule (RWTH) Aachen University, 52074 Aachen, Germany

7   Institute of Clinical Neuroscience and Medical Psychology, Medical Faculty, University of Düsseldorf, 40225 Düsseldorf, Germany

8   Department of Diagnostic and Interventional Radiology, Medical Faculty, University of Düsseldorf, 40225 Düsseldorf, Germany

9   Institute of Radiology and Neuroradiology, Evangelisches Krankenhaus, University of Oldenburg, 26129 Oldenburg, Germany

10   Department of Neuroscience, University Medical Center Groningen, University of Groningen, 9713 AV Groningen, The Netherlands

11   SCALab (CNRS UMR9193) & CHU de Lille, Hôpital Fontan, Pôle de Psychiatrie (CURE), Université de Lille, 59037 Lille, France

12   Departments of Neuroradiology, Nuclear Medicine and Neuroimaging Center, Technische Universität München, 80333 Munich, Germany

convergent organization of the striatum, representing a fundamental topographical model that can be useful for investigating structural and functional variability in aging and in clinical conditions.

Introduction

The striatum is a subcortical structure located close to the lateral ventricle and is anatomically composed of the putamen and the caudate. These two nuclei are anteriorly fused. Posteriorly, they become gradually separated by the internal capsule. The striatum receives diverse topographic projections from the cerebral cortex, which are mirrored by its structural and functional subdivisions, i.e., parcellations [1–3]. Accordingly, the striatum plays an important role in several motor and cognitive functions and is also involved in goal-directed behaviors, such as working memory, reward, and reinforcement learning [4–7]. In relation to its large functional involvement, alterations of the striatum are associated with highly prevalent and disabling pathologies in neurology and psychiatry, including Parkinson's disease (PD) and schizophrenia (SCZ) [8–11]. Therefore, identifying the fundamental subdivisions within the striatum that reflect both structural and functional aspects, thus establishing their behavioral and cognitive roles, and studying their alterations in clinical populations, is a major objective for cognitive and clinical neuroscience.

In-vivo and non-invasive neuroimaging modalities, such as resting-state functional magnetic resonance imaging (MRI) and diffusion MRI, provide connectivity measurements that capture modality-specific structural and/or functional neurobiological features of brain organization. The connectivity-based parcellation (CBP) approach can then be used to identify relatively homogenous subdivisions with regard to the investigated modality [12–17] (for a review, see Eickhoff, Thirion, Varoquaux, Bzdok [18]). Several such uni-modal parcellation studies have investigated the structural and functional subdivisions within the human striatum [2, 19, 20]. For example, probabilistic diffusion tractography (PDT) has been used to examine striatal organization based on the structural connectivity of multiple cortico-striatal pathways, revealing a differentiation along both the anterior-posterior and ventro-dorsal axes [2, 9]. Functional subdivisions of the striatum based on its resting-state functional connectivity (RSFC) to the entire brain highlighted a rostro-caudal and a ventro-dorsal organization [21, 22]. Pauli, O'Reilly, Yarkoni, Wager [7] examined the task-based functional co-activation patterns of striatal voxels with the cerebral cortex by applying a meta-analytic approach using 5,809 functional imaging studies. Based on these co-activation patterns, the striatum was divided into five subregions along the anterior-posterior axis. Taken together, the above studies have revealed a convergent ventral striatum subdivision, while the dorsal and caudal subdivisions seem to diverge across modalities (see Supplementary Introduction and Fig. S1). For example, the dorsal striatum was subdivided along the dorsal-ventral axis by RSFC-CBP [21, 23] or along the rostral-caudal axis by PDT-CBP [2]. The caudal striatum emerged as an entire cluster in RSFC-CBP [7, 21], but it was split into dorsal and ventral parts by PDT-CBP [2]. Although these studies have alluded to both similar and differing subdivisions in the striatum, it is much less clear to what extent these subdivisions converge across imaging modalities.

Given the diverse topographical organization, as well as the functional diversity of the striatum, multi-modal parcellation may provide a holistic "map" that reflects its fundamental biological heterogeneity as well as homogeneity. Importantly, such a multi-modal organization has the potential to reveal associations between the striatum and complex behaviors, as well as diseases, which are insufficiently explainable by a single modality alone. To the best of our knowledge, no other study has applied multi-modal parcellation to examine the structural and functional convergence of striatal clusters across modalities. Perhaps this is due to the current lack of suitable and reliable methods for obtaining multi-modal parcellations. One possibility is to derive multi-modal parcellations as a *post-hoc* combination of uni-modal maps. Several previous studies [16, 24–31] have applied a *post-hoc* approach to investigate the multi-modal organization of a brain region by studying the convergence and divergence between modality-specific parcellation, i.e. each modality is parcellated separately and the results are then combined to arrive at multi-modal parcellation. However, since such approaches do not explicitly model the dependencies between the modalities, they may result in a sub-optimal multi-modal parcellation [32].

In this study, we set out to investigate the multi-modal organization of the striatum, in order to reveal its fundamental biological map.

Materials and Methods

Sample Description

We assessed 324 unrelated subjects (164 females) aged 28.22 ± 3.88 years (mean ± standard deviation) from the young adult sample of the Human Connectome Project

(HCP) data [33]. This dataset was matched for gender frequency and age and had been used in our previous study [29]. Our sample did not contain siblings, as their presence might bias the results due to any similarity in functional and structural images. Three modalities of each subject – probabilistic diffusion tractography (PDT), RSFC and structural covariance (SC) – were used for the multi-modal parcellation of the striatum, as described below. We also selected another dataset of 220 unrelated subjects from the HCP and re-tested the multi-modal parcellation results (see Supplementary Results).

To analyze the clinical relevance, we collected the T1-weighted structural MRI data of PD patients from Heinrich Heine University Düsseldorf and Rheinisch-Westfälische Technische Hochschule Aachen University [34]. Together, these two datasets included 101 patients (47 females) aged 63.09 ± 10.06 years and 96 healthy controls (HC, 45 females) aged 58.87 ± 9.81 years. We also collected the T1-weighted structural MRI data of SCZ patients from the Center for Biomedical Research Excellence [35], the University of Groningen [36, 37], the University of Lille [38], the Technical University of Munich [39], and Utrecht University [40]. The pooled SCZ dataset included 159 patients (54 females) aged 35.92 ± 12.08 years and 166 HCs (64 females) aged 34.32 ± 11.94 years. There was no significant difference in gender between patients and HCs ($P = 0.96$, PD *versus* HC; $P = 0.39$ SCZ *vs* HC, χ^2 test). A significant difference was found in age between PD patients and HCs ($P < 0.01$, two-sample *t*-test), but not between SCZ patients and HCs ($P = 0.23$).

The ethics protocols were approved by the Ethics Committee of Heinrich Heine University Düsseldorf (4039 and 4096).

Region of Interest (ROI) Definition

The regions of interest (ROIs) for the left and right striatum were extracted using the Harvard-Oxford subcortical structural probabilistic atlas from the FMRIB (Functional Magnetic Resonance Imaging of the Brain) Software Library (https://fsl.fmrib.ox.ac.uk/fsl/fslwiki). We extracted the caudate and the putamen as 2-mm isotropic voxels based on the 25% probability map and combined them into one striatal ROI for each hemisphere. This procedure resulted in left and right striatum ROIs with 1,286 voxels (caudate: 487, putamen: 799) and 1,307 voxels (caudate: 511, putamen: 796), respectively. To investigate the robustness of the clustering results in ROI selection, we performed additional analyses using ROIs with a more conservative probability threshold of 50% (see Supplementary Results).

Connectivity Profiles for Each Modality

PDT: Following standard pre-processing in the FMRIB Software Library and BEDPOSTX fiber estimation, probabilistic tractography was used to generate 5,000 samples from each ROI voxel. Sample counts were recorded from the entire white matter in order to obtain a connectivity matrix per subject.

RSFC: Data were preprocessed using FMRIB's ICA-based Xnoiseifier (FIX), linear global signal regression (GSR), and band-pass filtering (0.01–0.08 Hz). The connectivity matrix for each subject was calculated as the Fisher-Z transformed Pearson correlation between the time-series of the ROI voxels with the rest of the grey matter (GM) voxels.

SC: T1 images were processed using the Computational Anatomy Toolbox (CAT12, http://www.neuro.uni-jena.de/cat/) with standard settings. The CAT12 is a toolbox extension to SPM12 and provides computational anatomy. We extracted the volume of each seed voxel (within the striatum) and other GM voxels for each subject. Pearson correlation was then applied across all subjects to generate connectivity matrices. Bootstrap re-sampling was applied 324 times to ensure robustness.

We averaged the PDT, RSFC (subject-wise), and SC (bootstrap-wise) connectivity matrices to generate one group-representative connectivity matrix per modality. Detailed information on pre-processing and connectivity matrix calculations is available in the Supplementary Methods.

Multi-modal CBP

Previous CBP studies [14, 27, 41] have used the popular *k*-means or hierarchical clustering methods to investigate the functional or structural parcellation of an ROI. First, each modality is used separately to arrive at a modality-specific (uni-modal) parcellation. These modality-specific parcellations are then combined or compared in a "*post-hoc*" fashion to arrive at a multi-modal solution. However, these methods do not explicitly model the dependencies among the modalities during the clustering process and thus may miss subtle similarities or differences between them. In this study, we explicitly modeled the dependencies among modalities using the context-dependent clustering (CDC) algorithm to investigate multi-modal CBP. CDC is an integrative clustering approach that takes the heterogeneity of the different contexts (i.e., modalities) into account by jointly modeling information from all the modalities during the clustering process and allows the connectivity of each modality to be of a different size. Thus, the three group-level connectivity matrices (RSFC, PDT, and SC) representing different modalities were used as the input for

CDC, yielding their single- and multi-modal clustering structure. To differentiate from the uni-modal parcellation, where clusters are independently generated for a given modality, here we used single-modal component parcellation (or single-modal parcellation for short) to denote the single-modality contribution to the multi-modal parcellation. We needed two additional parameters for CDC: the number of single-modal clusters and the maximum number of multi-modal clusters. In order to assess the effects of different levels of single-modal subdivision, we varied the number of components (n) in the range 3–9. The maximum number of multi-modal clusters should be high enough to accommodate heterogeneity across the modalities. Higher heterogeneity across modalities leads to more multi-modal clusters. We deemed 10 multi-modal clusters to be flexible enough, as previous studies have divided the striatum into 3–7 clusters in uni-modal parcellation.

The CDC algorithm uses a hierarchical Bayesian probabilistic model to jointly model the cluster structure by taking into account multiple contexts/modalities. Specifically, the Gaussian mixture model with the Dirichlet prior is used to model the components based on the corresponding connectivity patterns. The single-modal components themselves are modelled as Gaussian mixtures which are then combined to form multi-modal clusters using a hierarchical Bayesian model. Thus CDC can take data from multiple modalities as input; note that the connectivity patterns for different modalities can be of different sizes as long as they all have the same number of ROI voxels. The model is fitted using the Markov chain Monte Carlo (MCMC) algorithm. We used 2,000 MCMC iterations to allow convergence. CDC was applied to the left and right ROIs separately using the Clusternomics package (https://cran.r-project.org/web/packages/cluster nomics/index.html).

Model Selection

Selection of a clustering model is an unsolved problem, and many model-selection criteria exist. Thus, it is necessary to apply objective criteria to select a solution supported by the data [18]. Various selection criteria can disagree with each other and suggest different solutions, and it is not possible to know which criterion to prefer. Therefore, our model-selection was guided by a heuristic combination of several criteria. The matched clusters criterion (MCC), the deviance information criterion (DIC), the missing rate of voxels assigned to undersized clusters, and the adjusted Rand index (ARI) between single-modal clusters were used to select a parsimonious solution. All these criteria are described in more detail in the Supplementary Methods. In addition, results in the literature divide the striatum into five, six, or seven

clusters, suggesting that a plausible solution lies within this range. A hemisphere-matched parcellation was obtained by retaining only the matching voxels from the selected hemispheric parcellations (see Supplementary Methods).

Overall, multi-modal clusters from low to high levels of subdivision (n = 3–9) split the left striatum into rostro-caudal and ventro-dorsal clusters. After excluding small clusters (<50 voxels), we found seven multi-modal clusters at n = 3, 4, 7, and 8, eight multi-modal clusters at n = 5 and 6, and nine multi-modal clusters at n = 9. For the right striatum, we found a modal–modal cluster along the ventro-dorsal axis at low levels of subdivision (n = 3–6), and along the rostro-caudal and ventro-dorsal axes at high levels of subdivision (n = 7–9). We obtained six, seven, and eight multi-modal clusters at n = 3 and 9, n = 5 and 6, and n = 4, 7, and 8, respectively.

Functional Characterization of Striatal Clusters

We used the "behavioral domain" and "paradigm class" in the BrainMap meta-data (http://www.brainmap.org/index. html) [42, 43] to investigate the functions of the final hemisphere-matched multi-modal clusters in the striatum. The BrainMap meta-data describes more than 17,047 manually-curated neuroimaging experiments that have included the coordinates of peak voxels in active regions for specific psychological conditions. Behavioral domains include the categories of cognition, action, perception, emotion, interoception, and their related subcategories, while the paradigm classes categorize the specific task employed. We used "forward inference" and "reverse inference" to characterize the functional profile of each cluster.

Voxel-Based Morphometry (VBM) Analysis

To investigate clinically-relevant structural changes in PD and SCZ, we chose to analyze T1-weighted images, which are routinely collected in the clinic. This, in turn, increased the translational potential of our results.

T1-weighted images were first pre-processed using CAT12 with the same steps used for structural covariance connectivity (see Supplementary Methods). We estimated whole-brain GM volume by using only non-linear components of the deformation in normalized GM. For a given matched multi-modal cluster, we extracted the GM volume using VBM, which was then averaged within each cluster for each subject and examined for differences between patients and HCs. Considering that differences in GM volume might be associated with gender, age, and hemisphere, we applied a six-way analysis of variance (ANOVA) that included not only "disease status" and

"striatal cluster", but also "gender", "age", "hemisphere" and "total intracranial volume" as factors. In addition, for each striatal cluster, we calculated the Z-score of the averaged GM volume for each patient based on the mean and standard deviation of the HC group to further reflect specific and common structural alterations within and between PD and SCZ.

Results

CDC provides single-modal parcellations and their combination as multi-modal parcellation. We first describe the single-modal results at different numbers of components followed by the multi-modal results. Subsequently, a single solution (fixed number of single-modal subdivisions) was selected and functional characterization was applied to investigate the behavioral functions associated with each hemisphere-matched multi-modal cluster. We then examined the differences in the averaged GM volumes of these clusters between patients (PD and SCZ) and HCs using VBM.

Single-Modal (Component) Parcellation

Left Striatum

The left striatum was split into different single-modal components along the rostro-caudal and ventro-dorsal axes for all levels of subdivision (i.e., single-modal solution n from 3 to 9, Fig. 1, left). At $n = 3$, PDT subdivided the striatum along the rostro-caudal axis, while it was divided into dorsolateral, ventromedial, and caudal clusters by RSFC and SC. At $n = 4$, all modalities differentiated a rostral cluster from a dorsolateral cluster. The dorsolateral and rostral clusters were stable across all modalities. These two clusters were preserved by RSFC and SC at $n = 5$. However, the dorsolateral striatum was fused into a rostral cluster by PDT. In turn, the caudal striatum was split into dorsal and ventral parts by RSFC and SC. Similar rostral, dorsolateral, ventromedial, and caudal (including the dorsal and ventral parts) striatum divisions were also found in all modalities at $n = 6$.

At subsequent higher-level subdivisions ($n = 7$–9), we found more similarity across single-modal parcellations. At $n = 7$, a rostral, ventral, and caudal (dorsal and ventral part) striatum similar to $n = 6$ was obtained, as well as a dorsolateral striatum that was differentiated from the dorsal striatum in all modalities. At $n = 8$, the rostral striatum was divided along the dorsolateral-ventromedial axis by RSFC and SC, while only the ventromedial part of the rostral striatum was preserved by PDT. Compared to $n = 8$, we found these two dorsolateral and ventromedial parts to be

fused into an entire rostral striatum in all modalities at $n = 9$, while a more central cluster was differentiated from a caudal cluster (dorsal part) in all modalities.

Right Striatum

We found that all three modalities divided the right striatum along the ventro-dorsal axis at low levels of single-modal parcellation (Fig. 1, right). The dorsolateral cluster included almost the entire caudate, along with parts of the dorsal putamen from $n = 3$ to $n = 6$. We obtained caudal and ventral clusters with all three modalities at $n = 3$. At $n = 4$, the caudal striatum (from $n = 3$) was divided into separate parts in each modality. PDT differentiated a caudal striatum along the ventro-dorsal axis, while RSFC and SC subdivided this caudal striatum along the rostro-caudal axis. At $n = 5$, both RSFC and SC distinguished the dorsal and ventral striatum from the caudal striatum (from $n = 3$). At $n = 6$, we found a central cluster to be partly derived from the ventral striatum by all three modalities. Moreover, the dorsal and ventral parts of the caudal striatum were fused together and then slightly differentiated at the ventral part and at the dorsal part by both RSFC and SC.

At $n = 7$, all modalities distinguished the dorsal and rostral striatum from the large dorsolateral striatum at $n = 6$. The dorsal and caudal parts of the caudal striatum were found from $n = 5$ in RSFC and SC. At $n = 8$, a part of the central striatum (from $n = 7$) was fused with the dorsolateral striatum in all modalities. At $n = 9$, all modalities divided the caudate along the ventro-dorsal axis and the putamen along the rostro-caudal axis. Similar dorsolateral clusters (from $n = 7$) were found in SC.

Model Selection for Multi-modal CBP

Our aim was to select a model that represents the convergent organization of the striatum and to study the functional and clinical relevance of the resulting clusters. Different single-modal components (varying from 3 to 9) led to different multi-modal clustering results, making it necessary to select a single model (i.e., number of single-modal clusters). This model-selection was guided by the MCC, the DIC, the missing rate of voxels due to small clusters, and the ARI (Fig. 2).

Given that most previous uni-modal parcellations indicated a symmetric subdivision in the striatum [2, 7, 19, 21], using the MCC, we first investigated which level of single-modal subdivision generated multi-modal clusters with a high match between the left and right hemisphere clusters. A matching rate of at least 50% of mirrored voxels was considered a match for each cluster. Six multi-modal clusters matched with $n = 7$, while for $n = 5$ and 6, there
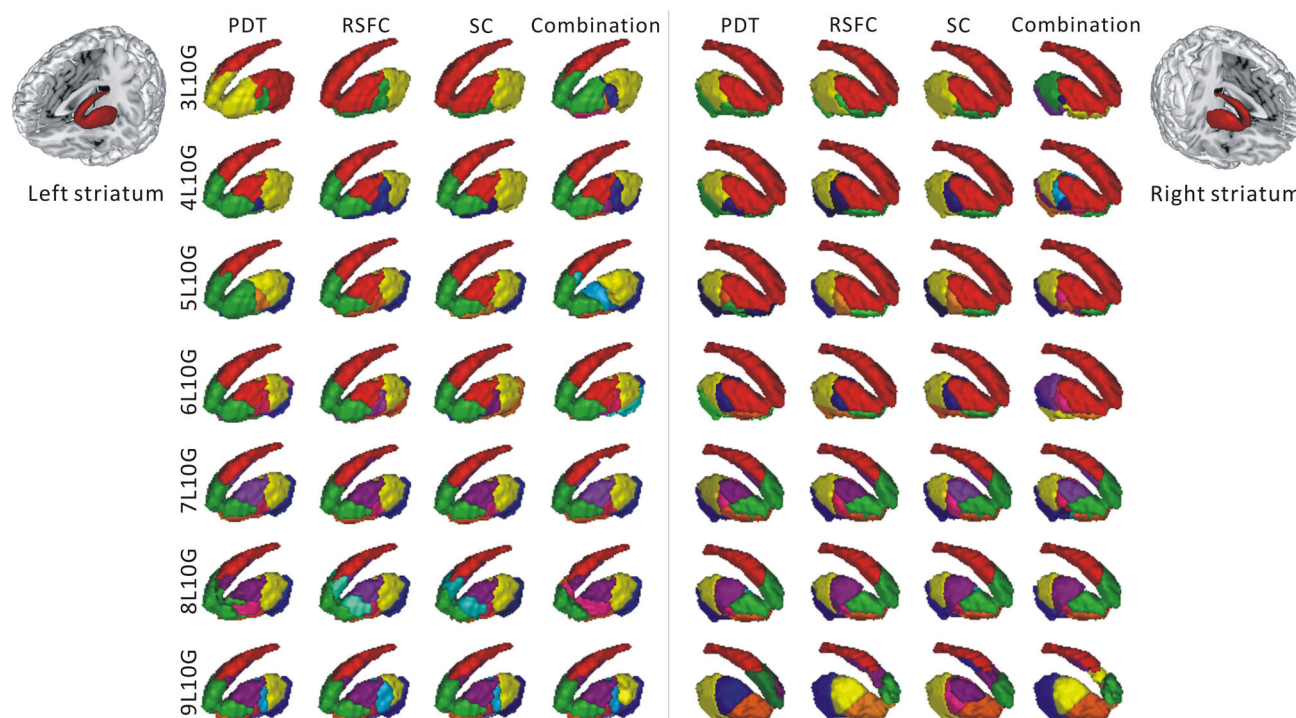
Fig. 1 Single- and multi-modal striatal clusters at different levels of subdivision (single-modal solution *n* from 3 to 9) and three modalities (PDT, RSFC, and SC). *PDT* probabilistic diffusion tractography, *RSFC* resting-state functional connectivity, *SC* structural covariance.

were only two and three matched multi-modal clusters, respectively. In addition, only a single cluster matched for *n* = 8. No multi-modal clusters met the MCC at *n* = 3, 4, and 9. Figure 2A shows the six matched multi-modal clusters at *n* = 7. More details about matched multimodal clusters can be found in Table S1 in the Supplementary materials.

The DIC results at each level of subdivision in both hemispheres are shown in Fig. 2B. We found that *n* = 9 for both the left and right striatum induced the minimum DIC value, which suggested that all single-modal components at this level of subdivision generated more convergent multi-modal clusters. However, many voxels were missing in the multimodal clusters due to small clusters (clusters with <50 voxels were deemed meaningless) at *n* = 9 (Fig. 2C). Furthermore, the averaged ARI across all pairwise modalities showed a peak at *n* = 8 and 9 for the left striatum, and *n* = 8 for the right striatum (Fig. 2D). At *n* = 7, the ARI showed a high correspondence. In addition, previous results have often divided the striatum into six clusters.

Taking all lines of evidence into account, and to retain maximum voxels in the striatal clusters, we determined *n* = 7 as our final model. The corresponding hemisphere-matched multi-modal clusters were selected for subsequent functional characterization and VBM analysis of clinical data. However, for completeness, we also discuss the results of *n* = 6 and 9.

Multi-modal CBP

All multi-modal clustering results for the left and right striatum are shown in Fig. 1. When using *n* = 7, we found seven multi-modal clusters with at least 50 voxels for the left striatum and eight for the right striatum (Fig. 3A). For both the left and right sides, we found dorsal (red), dorsolateral, rostral (green), ventral (orange), and caudal (ventral part, dark blue; dorsal part, yellow) subdivisions. We also found a central subdivision (pink) on the left side, which corresponded to a central (pink) and a ventromedial (light blue) cluster on the right side. Figure 3B shows matched voxels across hemispheres in these multi-modal clusters. Multi-modal parcellation results (at *n* = 7) for the left and right striatum are available through this link: https://github.com/Xiaojin-LIU/ MultiModalParcellationStriatumResults.

Functional Characterization of Striatal Clusters

We investigated the functional characterization of multi-modal striatal clusters obtained from the selected model at *n* = 7. After small-cluster exclusion, followed by inter-hemispheric matching, we used six clusters with matched voxels across hemispheres: dorsal, dorsolateral, rostral, ventral, and caudal (dorsal and ventral parts) (Fig. 3B). We
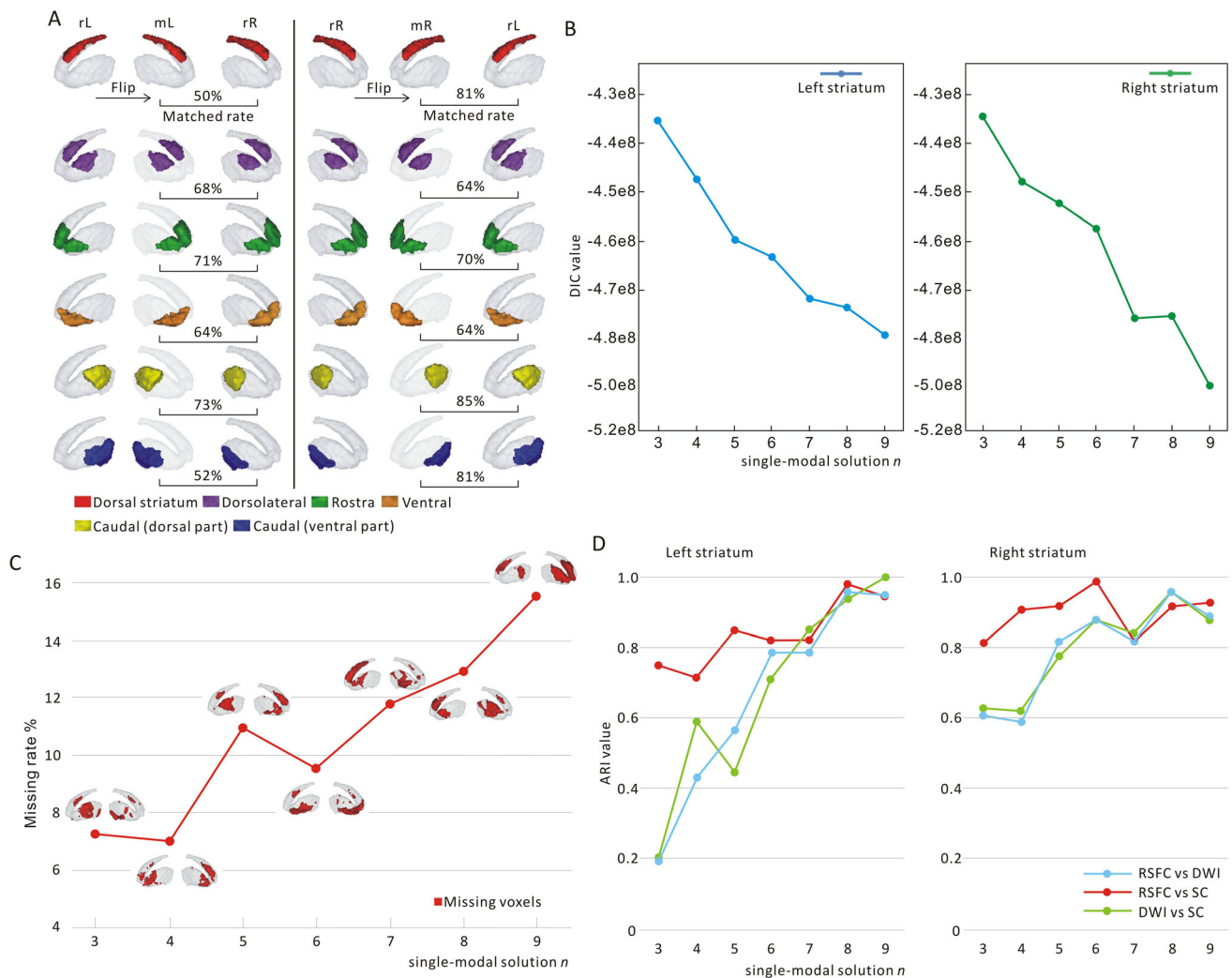
Fig. 2 **A** Matched rates between mirrored left cluster and real right cluster, and between mirrored right cluster and real left cluster for 6 hemisphere-matched multi-modal clusters at $n = 7$. **B** DIC values for different level subdivision (single-modal solution n from 3 to 9). **C** The missing rate of voxels in all multimodal clusters at different levels of subdivision (n from 3 to 9). The multi-modal clusters that combined PDT, RSFC (preprocessing strategy: FIX+lGSR), and SC single modalities. We only retained those meaningful multimodal clusters that contained at least 50 voxels [red voxels show the conjunction of all small (<50 voxels) clusters]. **D** Adjusted Rand index (ARI) between any two single modalities at different level subdivision (n from 3 to 9). *rL* real left cluster, *mL* mirrored left cluster, *rR* real right cluster, *mR* mirrored right cluster.

combined the left and right striatal clusters for this analysis.

Functional characterization across behavioral domains and paradigm classes of the BrainMap database showed the dorsolateral striatum to be associated with cognition and paradigms involving reward and saccades. The rostral and ventral striatum were both mainly associated with cognitive and emotional functions derived from relevant paradigms such as reward, Tower of London, and delay discounting (Fig. 4). Moreover, the ventral striatum was associated with perception and reward-processing. In contrast, the caudal striatum, including the dorsal and caudal putamen, was associated with executive action.

Clinical Assessment: GM Volume Alterations in PD and SCZ

We assessed how "disease status", "age", "gender", "striatal clusters", "hemisphere" and "total intracranial volume" affected the average GM volume of the striatum by applying six-way ANOVA.
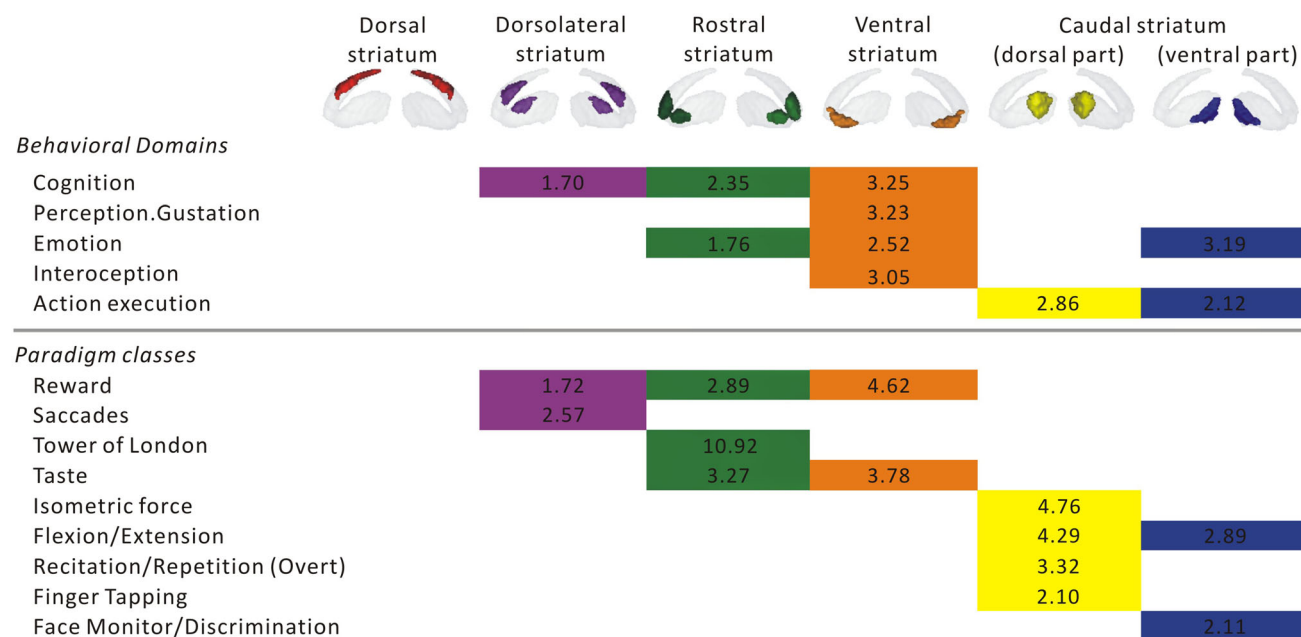
Main Effect

We found significant main effects of "disease status", "age", and "striatal cluster" on the average GM volume in both disorders (all $P < 0.001$) (Fig. 5A). Both PD and SCZ patients showed significantly lower GM striatal volumes
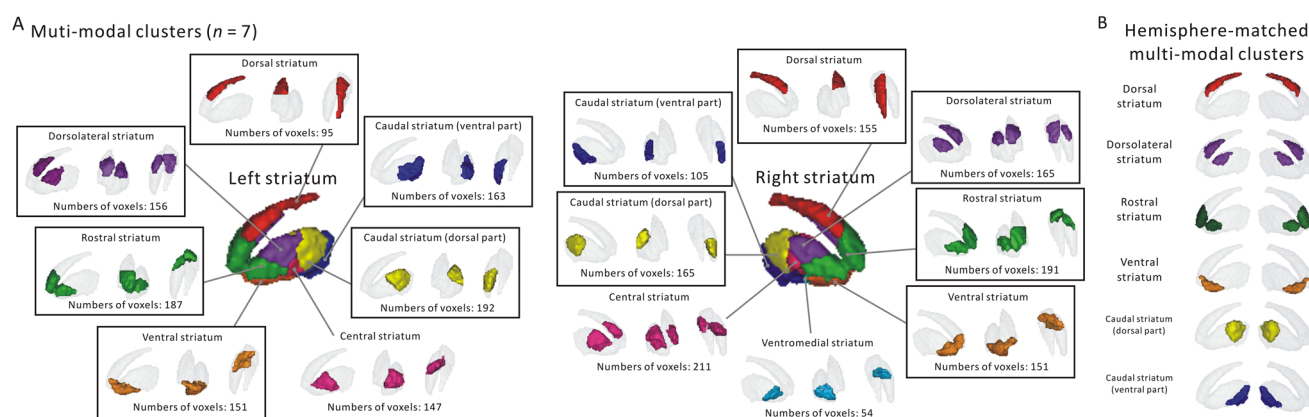
Fig. 3 Location and number of voxels of each multi-modal cluster at n = 7. **A** Selected highly-matched multi-modal clusters after retaining voxels that show a match across hemispheres (in black boxes). **B** Six hemisphere-matched multi-modal clusters at *n* = 7. Red, dorsal; purple, dorsolateral; green, rostral; orange, ventral; dark blue, caudal (ventral part); yellow, caudal (dorsal part); pink, central; light blue, ventromedial.

|	Dorsal striatum	Dorsolateral striatum	Rostral striatum	Ventral striatum	Caudal striatum (dorsal part)	Caudal striatum (ventral part)
Behavioral Domains						
Cognition		1.70	2.35	3.25		
Perception.Gustation				3.23		
Emotion			1.76	2.52		3.19
Interoception				3.05		
Action execution					2.86	2.12
Paradigm classes						
Reward		1.72	2.89	4.62		
Saccades		2.57				
Tower of London			10.92			
Taste			3.27	3.78		
Isometric force					4.76	
Flexion/Extension					4.29	2.89
Recitation/Repetition (Overt)					3.32	
Finger Tapping					2.10	
Face Monitor/Discrimination						2.11

Fig. 4 Behavioral decoding across behavioral domains and paradigm classes of the BrainMap database of the six hemisphere-matched multi-modal clusters at *n* = 7.

than HCs (all $P < 0.001$). Younger subjects had a higher GM volume than older subjects. We further found a significant negative correlation between the GM volume of the striatum and age (PD and HC: $r = -0.302$, $P < 0.001$; SCZ and HC: $r = -0.376$, $P < 0.001$). Moreover, males had a significantly higher GM volume than females ($P = 0.004$) when combining the SCZ and HC groups. The left hemispheric GM volume was found to be significantly higher than the right ($P = 0.034$) in HCs than in SCZ patients. Significant main effects of "total intracranial volume" on the average GM volume were only found in

SCZ patients and HCs ($P < 0.001$), but not in PD patients and HCs.

Interaction Effects

We then focused on the interaction effects of the factor "disease status" (PD and SCZ separately) (Fig. 5B–E). Significant interactions of "disease status" were found with all other factors ("striatal cluster", "age", "gender", and "hemisphere"). Resolving these interaction effects showed PD patients to have a lower average GM volume in the left dorsolateral ($P = 0.004$), rostral ($P = 0.021$), and ventral
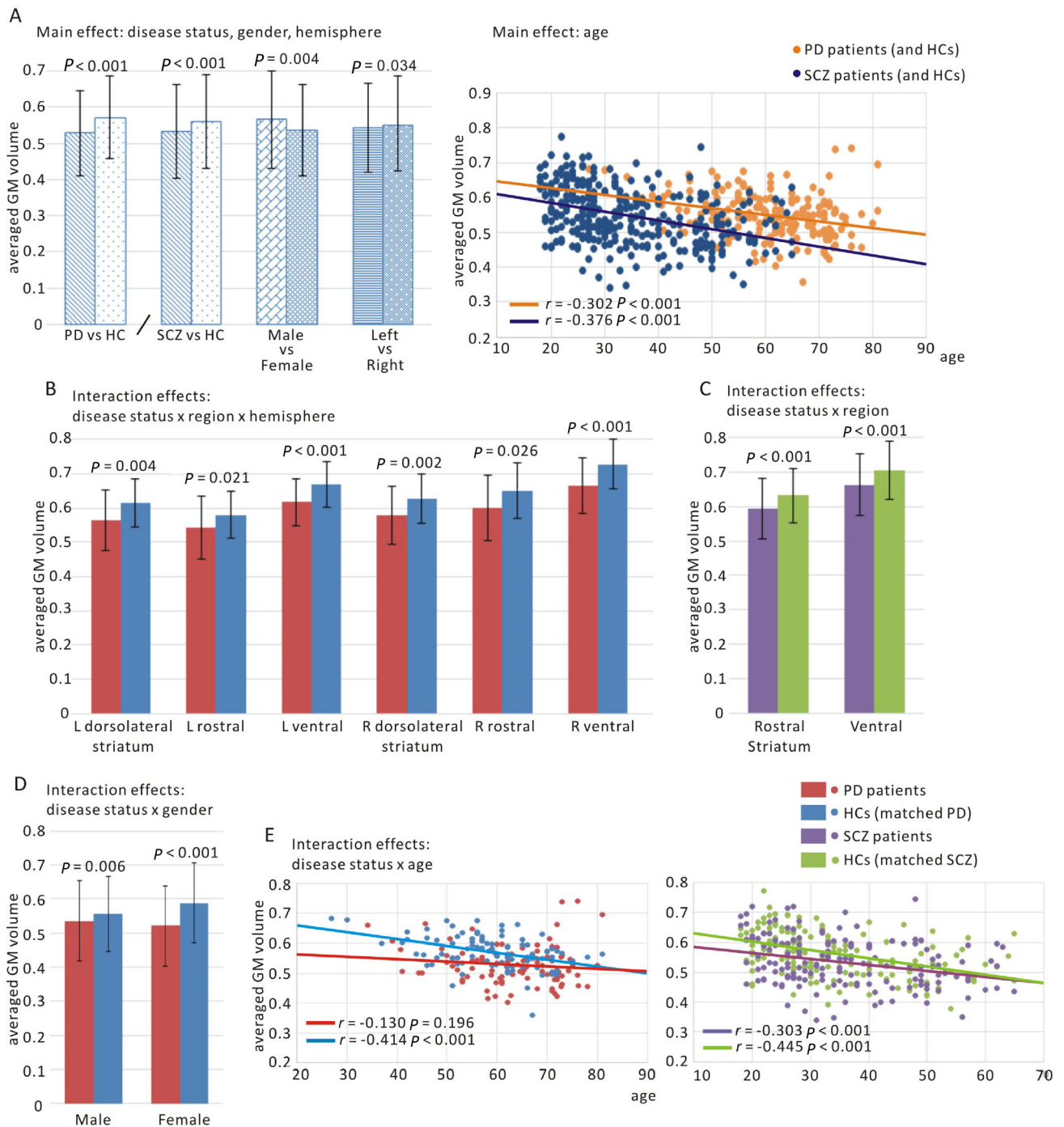
Fig. 5 Significant main (**A**) and interactive effects (**B–E**) in averaged grey matter (GM) volume of the striatum for PD patients and HCs, as well as SCZ patients and HCs based on ANOVA. *L* left hemisphere, *R* right hemisphere, *PD* Parkinson's disease, *SCZ* schizophrenia, *HCs* healthy controls.

striatum ($P < 0.001$) than HCs (Fig. 5B). Similar effects were also found in the same striatal clusters on the right hemisphere (Fig. 5B). However, a lower GM volume was found in the rostral ($P < 0.001$) and ventral striatum ($P < 0.001$) for SCZ patients (Fig. 5C). The interaction effect of "disease status" and "gender" showed both male ($P = $

0.006) and female ($P < 0.001$) PD patients to have a lower GM volume than HCs (Fig. 5D). We also found significant interactions between "disease status" and "age", showing a negative correlation between GM volume of the striatum and age in both SCZ patients ($r = -0.303$, $P < 0.001$) and HCs ($r = -0.445$, $P < 0.001$, Fig. 5E). The Z-scores of the

cluster-wise GM volume in PD and SCZ patients showed a uniformly lower Z-score for all hemisphere-matched clusters in the PD patients compared to the SCZ patients (Fig. 6). Note that all the Z-scores are negative, and a lower value denotes more atrophy.

Discussion

The primary goal of this study was to uncover the fundamental multi-modal organization of the striatum. We achieved this by using a novel multi-modal CBP approach that combined the RSFC, PDT, and SC modalities. The multi-modal CBP model based on seven single-modal clusters was selected based on several model-selection criteria. It revealed a ventro-dorsal and a rostro-caudal topographical organization of the striatum. According to this model, we identified six hemisphere-matched clusters: the dorsal, dorsolateral, rostral, ventral and caudal (dorsal and ventral part) striatum. Functional characterization of these striatal clusters, based on published activation studies, revealed their involvement in emotion, cognition, and execution. Critically, we found a reduced GM volume in the rostral and ventral striatum in both PD and SCZ patients, but GM volume reduction in the dorsolateral striatum was specifically attributable to PD patients.

Topographical Organization of the Striatum

We found a ventro-dorsal and rostro-caudal topographical organization of the striatum in both single-modal and multi-modal clusters (Fig. 1). The ventral striatal cluster from our final model was consistent with most previous functional and structural parcellations. Similar to previous RSFC-based parcellations, we found a rostral striatum that

includes the anterior caudate and putamen. A previous study [2] divided the dorsal striatum into three parts along the anterior-posterior axis based on its PDT-derived structural connectivity with the cerebral cortex. However, our results showed a dorsal striatal cluster across all modalities. The above results suggest a stable functionally and structurally convergent organization of the ventrodorsal and rostrocaudal striatum. In addition, we found a novel cluster (dorsolateral striatum) that combines two separate anatomical parts, one located in the ventral caudate and the other in the dorsolateral putamen. Our findings suggest functional and structural homogeneity between these two parts, which needs further investigation.

Convergent and Divergent Fundamental Organization of the Striatum

The convergence and divergence between the modalities for both the left and right striatum were found at all levels of subdivision. At lower levels ($n = 3$–6), we found divergent multi-modal clusters, while at higher levels ($n = 7$–9), more convergence was found. These clusters included dorsal, dorsolateral, rostral, ventral, central, and caudal (dorsal and ventral parts) clusters for the left striatum and an additional ventromedial cluster for the right striatum in multi-modal CBP (Fig. 3). A previous study [44] found that the rostral and dorsal striatum exhibit convergent structural and functional connectivity from orbitofrontal, lateral prefrontal, and posterior parietal regions of the cortex. Our multi-modal CBP results corroborate these two striatal regions (rostral and dorsal striatum), but also suggest that additional regions, including ventral, central, and caudal clusters, have a convergent functional and structural organization.
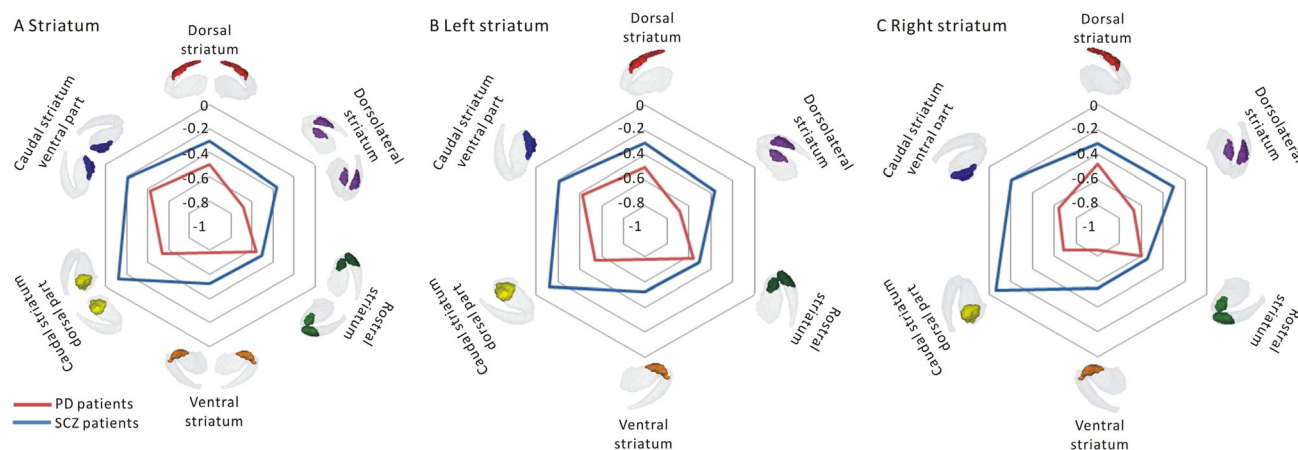
Fig. 6 Averaged Z-scores of GM volume in each striatal cluster for patients (PD and SCZ) by comparing the mean and standard deviation of the HC group. A Six hemisphere-matched multi-modal clusters. B, C Left (B) and right (C) striatal clusters. *PD* Parkinson's disease, *SCZ* schizophrenia.

Regarding the increasing functional and structural convergence of the striatum from a low to high level of subdivision, this may be related to single-modal components reflecting heterogeneous biological aspects of the striatum at the coarser level—i.e., few clusters resulting in divergent multi-modal clustering. Evidence [1, 3, 45] suggests that cortico-striatal projections are quite complex, forming an integrative functional circuit rather than being simple parallel pathways. This complexity may explain the increased multi-modal convergence at higher levels of subdivision.

Functional Characterization of Striatal Clusters

Activation studies based on functional behavioral profiling [43] of each symmetrical striatal cluster indicated that functions usually associated with the striatum include emotion, cognition, and action execution (Fig. 4). In particular, the dorsolateral striatum, including parts of the ventral caudate and dorsolateral putamen, were related to cognitive functions. The rostral and ventral striatal clusters were associated with commonly engaged behavioral functions, including cognition and emotion. The caudal striatum, including the dorsal and caudal parts, was associated with action. These results are in line with previous studies [46, 47], which have suggested that the ventral striatum is responsible for initiating behaviors and associated with emotion and motivation. Meanwhile, the caudate has been linked to cognitive functions, including procedural learning and working memory [48, 49], while the putamen has been associated mostly with action execution and motor control [50, 51]. The rostral striatum may be considered a "transitional" functional region that is responsible for different behavioral stages, including motivation and cognition. The striatum works in coordination with the cerebral cortex and is related to goal-directed behaviors [3, 52]. This complex behavior requires motivation at the beginning, followed by different cognitive functions, including a series of mental processes, such as memory, attention, imagination used to select a strategy, and finally, action. During these processes, individual emotions also play an important role because they affect strategy selection and can induce different behavioral results. Our functional characterization of the convergent striatal clusters obtained by multi-modal CBP is consistent with functions that can be expected of these regions. In order to further examine functional symmetry between hemispheres, we investigated the functional characterization of each striatal cluster on both sides, and found similar profiles for the left and right striatal clusters (Fig. S5).

Disease-Related Structural Differences in Striatal Clusters

We found main effects of "disease status", "age", and "hemisphere" on the average GM volume (Fig. 5A) in both disorders. Compared to HCs, patients showed a significantly lower GM volume of the entire striatum. These results are in line with previously identified morphological differences in these patient groups [53–56]. Currently, the pathology of PD is considered to be the degeneration of dopaminergic nigrostriatal neurons, which may result in the abnormal depletion of striatal dopamine [57]. In contrast, increased striatal dopamine activity is thought to be fundamental for SCZ [58, 59]. These may lead to divergent morphological differences in the striatum between PD and SCZ patients. In addition, most antipsychotic treatments target the dopaminergic receptors in the striatum and influence striatal metabolism in SCZ [60]. These treatments may also indirectly induce changes in striatal morphometry.

Significant interaction effects of "disease status" (PD and HC) with "striatal cluster" and "hemisphere" for the left and right dorsolateral, rostral, and ventral striatum (Fig. 5B) were found in this study. The GM volume of these striatal clusters was significantly lower in PD patients than in HCs. We also found a significant interaction effect of "disease status" (SCZ and HC) with "striatal cluster" for the rostral and ventral striatum when comparing SCZ patients and HCs (Fig. 5C). These results suggested that significant structural atrophy in the rostral and ventral striatum is common to both PD and SCZ patients, but a difference in the dorsolateral striatum is specifically attributable to PD patients. Structural alterations in prefrontal, striatal, and temporal regions are associated with the symptoms of these two disorders [61–64]. The most common symptoms of PD and SCZ are cognitive impairment, emotional distress, and slowing of movements [65]. This symptomatic similarity between PD and SCZ may stem from dopamine dysregulation of striatal clusters, which, in turn, can lead to reduced spontaneity and initiative, hence difficulties in the planning, selection, initiation, and execution of movements. Given that the functional characterization of the rostral and ventral striatum was mainly associated with complex functions [not only cognition but also emotion (Fig. 4)], dysfunctions of these two striatal clusters may induce common structural atrophy in PD and SCZ. However, significant structural atrophy in the dorsolateral striatum was found only in PD patients, reflecting a divergent atrophy pattern between PD and SCZ. A gradual decrease of dopaminergic function within the putamen from posterior to anterior has been described in PD [66, 67]. This may lead to PD-specific structural atrophy in the dorsolateral striatum, as we found

in this study. Also, different atrophy patterns may be related to the differences in predominant symptoms between PD and SCZ. The functional characterization of these two clusters showed them to be involved in cognition and action, respectively (Fig. 4). In particular, PD is considered a movement disorder, the predominant clinical symptoms of which include resting tremor, slowed movement, and postural disturbance [68, 69], while SCZ is a severe mental disorder and its negative symptoms predominantly involve abnormal motivation, sociality, and emotional expressiveness [70, 71]. PD patients are often diagnosed with mild cognitive impairment or dementia in different stages. This may explain the more extensive structural atrophy in the striatal clusters involved in action and cognition. Meanwhile, it has been shown that cortico-striatal connectivity with the posterior putamen, which mainly involves sensorimotor and executive networks, is decreased in PD, while cortico-striatal connectivity with the anterior putamen that mainly connects to the salience network is increased [72, 73]. Our findings are consistent with these studies, which suggest that abnormal executive and cognitive functions in PD may be associated with specific structural atrophy in relevant striatal clusters.

In addition, we found more lateralized atrophy in all the striatal clusters for PD patients compared to SCZ patients. Previous studies [74, 75] have suggested a predominance of nigrostriatal dysfunction in the left hemisphere for PD patients, which may lead to the "hemisphere" effect on GM volume for PD patients (Fig. 5B). The dorsolateral striatum (the novel cluster identified in our study) showed significant lateralized atrophy in PD patients compared to HCs, but no significant difference between SCZ patients and HCs. Hence, we suggest that this cluster may reflect a clinically relevant marker for PD but not for SCZ. Taken together, these results reflect the structure and function of our multi-modally derived striatal clusters corresponding to complex behaviors of clinical relevance. These convergent striatal clusters can thus be applied when investigating the structural and functional variability in PD and SCZ.

We found the GM volume of striatal clusters to be significantly lower in both male and female PD patients than in HCs (Fig. 5D). Also, there was no significant correlation between the GM volume of striatal clusters and age in PD (Fig. 5E). Although we are not aware of previous reports on differences in striatal GM volume and its relation to age and gender, these two factors are well-known clinical characteristics of PD [76]. In PD, females usually show greater striatal dopamine transporter activity along with a more rapid age-related decline than males [77]. Hence, we cautiously suggest an effect of age and gender on the difference in GM volume between PD patients and HCs. However, we found a significant negative correlation between the GM volume of striatal

clusters and age in SCZ (Fig. 5E). This may relate to the difference in the first-episode age of these two diseases. While the first episode in SCZ usually includes a wider age range—from the adolescent to the aged—PD normally affects the aged.

In summary, we revealed a convergent fundamental organization of the striatum using a novel multi-modal CBP approach. The dorsolateral cluster was related to cognition, the rostral and ventral clusters were associated with emotion and cognition, and the caudal cluster (dorsal and ventral parts) was related to the execution of actions. We also found common structural atrophy (GM volume) in the rostral and ventral striatum for PD and SCZ, but the GM differences in the dorsolateral striatum were specifically attributable to PD. In effect, we provide a parcellation scheme that can be used to congruously investigate the functional and structural variation of striatal clusters across development, aging, and disease.

Conflict of interest The authors claim that there are no conflicts of interest.

References

1. Alexander GE, DeLong MR, Strick PL. Parallel organization of functionally segregated circuits linking basal ganglia and cortex. Ann Rev Neurosci 1986, 9: 357–381.
2. Tziortzi AC, Haber SN, Searle GE, Tsoumpas C, Long CJ, Shotbolt P, *et al.* Connectivity-based functional analysis of dopamine release in the striatum using diffusion-weighted MRI and positron emission tomography. Cereb Cortex 2013, 24: 1165–1177.
3. Haber SN. The primate basal ganglia: parallel and integrative networks. J Chem Neuroanat 2003, 26: 317–330.
4. Balleine BW, Delgado MR, Hikosaka O. The role of the dorsal striatum in reward and decision-making. J Neurosci 2007, 27: 8161–8165.
5. Lewis SJ, Dove A, Robbins TW, Barker RA, Owen AM. Striatal contributions to working memory: a functional magnetic resonance imaging study in humans. Eur J Neurosci 2004, 19: 755–760.
6. Postuma RB, Dagher A. Basal ganglia functional connectivity based on a meta-analysis of 126 positron emission tomography and functional magnetic resonance imaging publications. Cereb Cortex 2005, 16: 1508–1521.
7. Pauli WM, O'Reilly RC, Yarkoni T, Wager TD. Regional specialization within the human striatum for diverse psychological functions. Proc Natl Acad Sci U S A 2016, 113: 1907–1912.
8. Schlagenhauf F, Huys QJ, Deserno L, Rapp MA, Beck A, Heinze H-J, *et al.* Striatal dysfunction during reversal learning in

unmedicated schizophrenia patients. Neuroimage 2014, 89: 171–180.

9. Singh A, Mewes K, Gross RE, DeLong MR, Obeso JA, Papa SM. Human striatal recordings reveal abnormal discharge of projection neurons in Parkinson's disease. Proc Natl Acad Sci U S A 2016, 113: 9629–9634.

10. Chen X, Xue B, Wang J, Liu H, Shi L, Xie J. Potassium Channels: a potential therapeutic target for parkinson's disease. Neurosci Bull 2018, 34: 341–348.

11. Song N, Xie J. Iron, dopamine, and α-synuclein interactions in at-risk dopaminergic neurons in Parkinson's disease. Neurosci Bull 2018, 34: 382–384.

12. Xu J, Wang J, Fan L, Li H, Zhang W, Hu Q, *et al.* Tractography-based parcellation of the human middle temporal gyrus. Sci Rep 2015, 5: 18883.

13. Zhang W, Wang J, Fan L, Zhang Y, Fox PT, Eickhoff SB, *et al.* Functional organization of the fusiform gyrus revealed with connectivity profiles. Hum Brain Mapp 2016, 37: 3003–3016.

14. Genon S, Li H, Fan L, Müller VI, Cieslik EC, Hoffstaedter F, *et al.* The right dorsal premotor mosaic: organization, functions, and connectivity. Cereb Cortex 2017, 27: 2095–2110.

15. Eickhoff SB, Yeo BT, Genon S. Imaging-based parcellations of the human brain. Nat Rev Neurosci 2018, 19: 672–686.

16. Plachti A, Eickhoff SB, Hoffstaedter F, Patil KR, Laird AR, Fox PT, *et al.* Multimodal parcellations and extensive behavioral profiling tackling the hippocampus gradient. Cereb Cortex 2019, 29: 4595–4612.

17. Reuter N, Genon S, Masouleh SK, Hoffstaedter F, Liu X, Kalenscher T, *et al.* CBPtools: a Python package for regional connectivity-based parcellation. Brain Struct Funct 2020, 225: 1261–1275.

18. Eickhoff SB, Thirion B, Varoquaux G, Bzdok D. Connectivity-based parcellation: Critique and implications. Hum Brain Mapp 2015, 36: 4771–4792.

19. Jung WH, Jang JH, Park JW, Kim E, Goo EH, Im OS, *et al.* Unravelling the intrinsic functional organization of the human striatum: a parcellation and connectivity study based on resting-state fMRI. PLoS One 2014, 9: e106768.

20. Draganski B, Kherif F, Klöppel S, Cook PA, Alexander DC, Parker GJ, *et al.* Evidence for segregated and integrative connectivity patterns in the human basal ganglia. J Neurosci 2008, 28: 7143–7152.

21. Janssen RJ, Jylänki P, Kessels RP, van Gerven MA. Probabilistic model-based functional parcellation reveals a robust, fine-grained subdivision of the striatum. Neuroimage 2015, 119: 398–405.

22. Jaspers E, Balsters JH, Kassraian Fard P, Mantini D, Wenderoth N. Corticostriatal connectivity fingerprints: Probability maps based on resting-state functional connectivity. Hum Brain Mapp 2017, 38: 1478–1491.

23. Choi EY, Yeo BT, Buckner RL. The organization of the human striatum estimated by intrinsic functional connectivity. J Neurophysiol 2012, 108: 2242–2263.

24. Kelly C, Toro R, Di Martino A, Cox CL, Bellec P, Castellanos FX, *et al.* A convergent functional architecture of the insula emerges across imaging modalities. Neuroimage 2012, 61: 1129–1142.

25. Wang J, Yang Y, Fan L, Xu J, Li C, Liu Y, *et al.* Convergent functional architecture of the superior parietal lobule unraveled with multimodal neuroimaging approaches. Hum Brain Mapp 2015, 36: 238–257.

26. Wang J, Zhang J, Rong M, Wei X, Zheng D, Fox PT, *et al.* Functional topography of the right inferior parietal lobule structured by anatomical connectivity profiles. Hum Brain Mapp 2016, 37: 4316–4332.

27. Xia X, Fan L, Cheng C, Eickhoff SB, Chen J, Li H, *et al.* Multimodal connectivity-based parcellation reveals a shell-core

28. Wang J, Xie S, Guo X, Becker B, Fox PT, Eickhoff SB, *et al.* Correspondent functional topography of the human left inferior parietal lobule at rest and under task revealed using resting-state fMRI and coactivation based parcellation. Hum Brain Mapp 2017, 38: 1659–1675.

29. Genon S, Reid A, Li H, Fan L, Müller VI, Cieslik EC, *et al.* The heterogeneity of the left dorsal premotor cortex evidenced by multimodal connectivity-based parcellation and functional characterization. Neuroimage 2018, 170: 400–411.

30. Xu J, Lyu H, Li T, Xu Z, Fu X, Jia F, *et al.* Delineating functional segregations of the human middle temporal gyrus with resting-state functional connectivity and coactivation patterns. Hum Brain Mapp 2019, 40: 5159–5171.

31. Wang J, Becker B, Wang L, Li H, Zhao X, Jiang T. Corresponding anatomical and coactivation architecture of the human precuneus showing similar connectivity patterns with macaques. NeuroImage 2019, 200: 562–574.

32. Gabasova E, Reid J, Wernisch L. Clusternomics: Integrative context-dependent clustering for heterogeneous datasets. PLoS Comp Biol 2017, 13: e1005781.

33. Van Essen DC, Smith SM, Barch DM, Behrens TE, Yacoub E, Ugurbil K, *et al.* The WU-Minn human connectome project: an overview. Neuroimage 2013, 80: 62–79.

34. Pläschke RN, Cieslik EC, Müller VI, Hoffstaedter F, Plachti A, Varikuti DP, *et al.* On the integrity of functional brain networks in schizophrenia, Parkinson's disease, and advanced age: Evidence from connectivity-based single-subject classification. Hum Brain Mapp 2017, 38: 5845–5858.

35. Mayer AR, Ruhl D, Merideth F, Ling J, Hanlon FM, Bustillo J, *et al.* Functional imaging of the hemodynamic sensory gating response in schizophrenia. Hum Brain Mapp 2013, 34: 2302–2312.

36. Vercammen A, Knegtering H, den Boer JA, Liemburg EJ, Aleman A. Auditory hallucinations in schizophrenia are associated with reduced functional connectivity of the temporo-parietal area. Biol psychiatry 2010, 67: 912–918.

37. Chen J, Patil KR, Weis S, Sim K, Nickl-Jockschat T, Zhou J, *et al.* Neurobiological divergence of the positive and negative schizophrenia subtypes identified on a new factor structure of psychopathology using non-negative factorization: an international machine learning study. Biol psychiatry 2020, 87: 282–293.

38. Lefebvre S, Demeulemeester M, Leroy A, Delmaire C, Lopes R, Pins D, *et al.* Network dynamics during the different stages of hallucinations in schizophrenia. Hum Brain Mapp 2016, 37: 2571-2586.

39. Peters H, Riedl V, Manoliu A, Scherr M, Schwerthöffer D, Zimmer C, *et al.* Changes in extra-striatal functional connectivity in patients with schizophrenia in a psychotic episode. Br J Psychiatry 2017, 210: 75–82.

40. Clos M, Diederen KM, Meijering AL, Sommer IE, Eickhoff SB. Aberrant connectivity of areas for decoding degraded speech in patients with auditory verbal hallucinations. Brain Struct Funct 2014, 219: 581–594.

41. Bzdok D, Heeger A, Langner R, Laird AR, Fox PT, Palomero-Gallagher N, *et al.* Subspecialization in the human posterior medial cortex. Neuroimage 2015, 106: 55–71.

42. Eickhoff SB, Bzdok D, Laird AR, Roski C, Caspers S, Zilles K, *et al.* Co-activation patterns distinguish cortical modules, their connectivity and functional differentiation. Neuroimage 2011, 57(3): 938–949.

43. Genon S, Reid A, Langner R, Amunts K, Eickhoff SB. How to characterize the function of a brain region. Trends Cogn Sci 2018, 22: 350–364.

44. Jarbo K, Verstynen TD. Converging structural and functional connectivity of orbitofrontal, dorsolateral prefrontal, and posterior parietal cortex in the human striatum. J Neurosci 2015, 35: 3865–3878.

45. Groenewegen HJ, Wright CI, Beijer AV, Voorn P. Convergence and segregation of ventral striatal inputs and outputs. Ann N Y Acad Sci 1999, 877: 49–63.

46. Cardinal RN, Parkinson JA, Hall J, Everitt BJ. Emotion and motivation: the role of the amygdala, ventral striatum, and prefrontal cortex. Neurosci Biobehav Rev 2002, 26: 321–352.

47. Pessoa L. How do emotion and motivation direct executive control? Trends Cogn Sci 2009, 13: 160–166.

48. Grahn JA, Parkinson JA, Owen AM. The cognitive functions of the caudate nucleus. Prog Neurobiol 2008, 86: 141–155.

49. Robinson JL, Laird AR, Glahn DC, Blangero J, Sanghera MK, Pessoa L, et al. The functional connectivity of the human caudate: an application of meta-analytic connectivity modeling with behavioral filtering. Neuroimage 2012, 60: 117–129.

50. Marchand WR, Lee JN, Thatcher JW, Hsu EW, Rashkin E, Suchy Y, et al. Putamen coactivation during motor task execution. Neuroreport 2008, 19: 957–960.

51. Marchand WR, Lee JN, Suchy Y, Garn C, Chelune G, Johnson S, et al. Functional architecture of the cortico-basal ganglia circuitry during motor task execution: Correlations of strength of functional connectivity with neuropsychological task performance among female subjects. Hum Brain Mapp 2013, 34: 1194–1207.

52. Grace AA, Floresco SB, Goto Y, Lodge DJ. Regulation of firing of dopaminergic neurons and control of goal-directed behaviors. Trends Neurosci 2007, 30: 220–227.

53. Jia X, Liang P, Li Y, Shi L, Wang D, Li K. Longitudinal study of gray matter changes in Parkinson disease. Am J Neuroradiol 2015, 36: 2219–2226.

54. Xu Y, Yang J, Hu X, Shang H. Voxel-based meta-analysis of gray matter volume reductions associated with cognitive impairment in Parkinson's disease. J Neurol 2016, 263: 1178–1187.

55. Fornito A, Yücel M, Patti J, Wood S, Pantelis C. Mapping grey matter reductions in schizophrenia: an anatomical likelihood estimation analysis of voxel-based morphometry studies. Schizophrenia Res 2009, 108: 104–113.

56. Torres US, Duran FL, Schaufelberger MS, Crippa JA, Louzã MR, Sallet PC, et al. Patterns of regional gray matter loss at different stages of schizophrenia: a multisite, cross-sectional VBM study in first-episode and chronic illness. NeuroImage 2016, 12: 1–15.

57. Dauer W, Przedborski S. Parkinson's disease: mechanisms and models. Neuron 2003, 39: 889-909.

58. Kapur S, Mizrahi R, Li M. From dopamine to salience to psychosis—linking biology, pharmacology and phenomenology of psychosis. Schizophrenia Res 2005, 79: 59–68.

59. Laruelle M, Abi-Dargham A. Dopamine as the wind of the psychotic fire: new evidence from brain imaging studies. J Psychopharmacology 1999, 13: 358–371.

60. Holcomb HH, Cascella NG, Thaker GK, Medoff DR. Functional sites of neuroleptic drug action in the human brain: PET/FDG studies with and without haloperidol. Am J Psychiatry 1996, 153: 41–49.

61. Nagano-Saito A, Washimi Y, Arahata Y, Kachi T, Lerch J, Evans A, et al. Cerebral atrophy and its relation to cognitive impairment in Parkinson disease. Neurology 2005, 64: 224–229.

62. Baggio H, Segura B, Ibarretxe-Bilbao N, Valldeoriola F, Marti M, Compta Y, et al. Structural correlates of facial emotion recognition deficits in Parkinson's disease patients. Neuropsychologia 2012, 50: 2121–2128.

63. Padmanabhan JL, Tandon N, Haller CS, Mathew IT, Eack SM, Clementz BA, et al. Correlations between brain structure and symptom dimensions of psychosis in schizophrenia, schizoaffective, and psychotic bipolar I disorders. Schizophrenia Bull 2014, 41: 154–162.

64. Hasan A, Wobrock T, Guse B, Langguth B, Landgrebe M, Eichhammer P, et al. Structural brain changes are associated with response of negative symptoms to prefrontal repetitive transcranial magnetic stimulation in patients with schizophrenia. Mol Psychiatry 2017, 22: 857–864.

65. Winograd-Gurvich C, Fitzgerald P, Georgiou-Karistianis N, Bradshaw J, White O. Negative symptoms: a review of schizophrenia, melancholic depression and Parkinson's disease. Brain Res Bull 2006, 70: 312–321.

66. Brooks DJ, Pavese N. Imaging biomarkers in Parkinson's disease. Prog Neurobiol 2011, 95: 614–628.

67. Goldstein D, Sullivan P, Holmes C, Kopin I, Basile M, Mash DC. Catechols in post-mortem brain of patients with Parkinson disease. Euro J Neurol 2011, 18: 703–710.

68. Jankovic J. Parkinson's disease: clinical features and diagnosis. J Neurol Neurosurg Psychiatry 2008, 79: 368–376.

69. Jankovic J, Tolosa E. Parkinson's Disease and Movement Disorders. Lippincott Williams & Wilkins, Philadelphia, 2007.

70. Brüne M. Emotion recognition,'theory of mind,'and social behavior in schizophrenia. Psychiatry Res 2005, 133: 135–147.

71. Pickup GJ, Frith CD. Theory of mind impairments in schizophrenia: symptomatology, severity and specificity. Psychol Med 2001, 31: 207–220.

72. Helmich RC, Derikx LC, Bakker M, Scheeringa R, Bloem BR, Toni I. Spatial remapping of cortico-striatal connectivity in Parkinson's disease. Cereb Cortex 2009, 20: 1175–1186.

73. Hacker CD, Perlmutter JS, Criswell SR, Ances BM, Snyder AZ. Resting state functional connectivity of the striatum in Parkinson's disease. Brain 2012, 135: 3699–3711.

74. Scherfler C, Seppi K, Mair KJ, Donnemiller E, Virgolini I, Wenning GK, et al. Left hemispheric predominance of nigrostriatal dysfunction in Parkinson's disease. Brain 2012, 135: 3348–3354.

75. Prakash BD, Sitoh Y-Y, Tan LC, Au WL. Asymmetrical diffusion tensor imaging indices of the rostral substantia nigra in Parkinson's disease. Parkinsonism Relat Disord 2012, 18: 1029–1033.

76. Miller IN, Cronin-Golomb A. Gender differences in Parkinson's disease: clinical characteristics and cognition. Move Disord 2010, 25: 2695–2703.

77. Lee JJ, Ham JH, Lee PH, Sohn YH. Gender differences in age-related striatal dopamine depletion in Parkinson's disease. J Move Disord 2015, 8: 130–135.